# HYDRODYNAMIC EROSION OF COPPER WITH DIFFERENT GRAIN SIZES

**ALICE CHLUPOVA[1], JAKUB POLOPRUDSKY[1], AKASH NAG[2], GABRIEL STOLARIK[3*]**

[1]Institute of Physics of Materials, Czech Academy of Sciences, Brno, Czech Republic,
[2]VSB - Technical University of Ostrava, Ostrava, Czech Republic
[3]Faculty of Manufacturing Technologies, TUKE, with a seat in Presov, Slovak Republic

**DOI: 10.17973/MMSJ.2025_10_2025097**
***Corresponding author: gabriel.stolarik@tuke.sk**

The evolution of water droplet erosion on copper with varying grain sizes altered by heat treatment was investigated. An ultrasonically driven pulsating water jet was employed as a droplet generator. The water jet treatment was performed at a frequency of 40 kHz using two levels of supply pressure of 20 and 30 MPa. The measurements of removed volume and achieved depth show a critical interplay between droplet-surface interaction development and material properties, including hardness, grain size, and plasticity. Two distinct erosion phenomena were observed, influenced by the effective interaction governed by the feed rates of the PWJ with the material. At the lowest feed rate (0.5 mm/s), the erosion resistance of the material modestly increased with the intensity of heat treatment for both levels of supply pressure. Suggesting plasticity is the main factor of erosion resistance. The largest mean depth was recorded in the basic state of the material (without heat treatment), namely 90.06 µm at a pressure of 20 MPa, and the minimum value was 42.23 µm at the highest heat treatment of 900°C/1h with a pressure of 30 MPa. This contrasts with the behaviour at the higher feed rate (0.67 mm/s), where more severe erosion with heat treatment intensity was observed. The hardness decreases and grain size increase caused by heat treatment intensity are the driving factors of erosion resistance at this feedrate. In this case, the lowest mean depth of 69.46 µm was observed in the basic heat-untreated state of the material at a pressure of 20 MPa, and the maximum mean depth of 103.17 µm at 30 MPa was observed in the treated sample at 900°C/1h. The results demonstrated different erosion responses of the material after its heat treatment depending on the change in the input feed rates. These findings contribute to a deeper understanding of the mechanisms of PWJ-induced erosion when interacting with materials of different hardness and grain size.

**KEYWORDS**

pulsating water jet, copper erosion, grain size, annealing, electron microscopy, fractography

## 1 INTRODUCTION

The erosion caused by the impact of liquid droplets is a constant subject of attention. Researchers aim to understand the fundamental mechanisms of how droplets interact with surfaces at high velocities [Bowden 1958], which involves studying the fluid dynamics [Nastic 2023], the properties of the impacted materials [Hloch 2022], and the conditions under which erosion occurs [Marzbali 2023]. It includes developing models to predict erosion behavior [Fujisawa 2022], [Fujisawa 2023]. Extensive research is being carried out on the impact of water droplets on materials with varying mechanical properties [Choi 2015]. The fundamental mechanism by which water droplets impact a material has been elucidated, primarily based on the approximate concept known as the hammer effect [Cook 1928]. Impact pressure $p_i$, often called the "hammer effect," is derived from the momentum of a droplet with a specific density $v \cdot \rho$. Upon collision, the droplet generates an acoustic wave $C$ that propagates into the interior of the solid. The speed of this acoustic wave, $C$, depends on the droplet's impact velocity $v$ (mm/s). When the droplet impacts at a speed of around 500 m/s, the speed of the acoustic wave can range from 2600 to 3000 m/s [Haller 2002]. The impact of water droplets over time leads to structural changes in both the surface and subsurface regions of the material. These changes are a compromise between the kinematic properties of the water droplets and the mechanical properties of the material [Hloch 2024]. Mechanical properties, such as hardness, toughness, and elasticity [Ahmad 2009], play a key role in determining how a material responds to the repeated impact of water droplets. For instance, materials with higher hardness can resist surface deformation better, but they might be more prone to brittle fracture under high-velocity impacts. Conversely, materials with higher toughness can absorb more energy from the impacts, reducing the likelihood of cracking but potentially leading to more significant surface wear over time [Nastic 2023]. These factors thus influence the ability of the material to resist damage caused by multiple impact pressure loads. Its resistance is a prerequisite for the development of individual erosion stages [Kamkar 2013]. It was shown that knowledge of the development of erosion is important for determining the erosion resistance of materials [Ahmad 2009], or conversely, to influence surface residual stresses [Siahpour 2022] or roughness [Stolarik 2023]. In several cases, a relatively high penetration ability of water droplets was found, which may be related to the frequency of water droplet impacts per unit time [Hloch 2022], [Chlupova 2023]. The influence of the solid surface in droplet impingement involves several specific features, such as initial roughness, erosion-induced roughness, hardness, and grain size. The size of material grains significantly influences the dynamics of the erosion process. Under high-frequency water droplet impacts, the resulting impact pressure can cause the upper region of the grains to deform from their equilibrium positions. The exposed grains can then be further influenced by another erosion factor: lateral jetting. Although the radius of action for lateral jetting is small [Fujisawa 2022], its speed is three to ten times faster than the droplet impact speed [Haller 2003]. This can lead to the shearing of these grains [Poloprudsky 2024] or water penetration into microcracks, creating micro-tunnels [Hloch 2022]. For this reason, the possible influence of grain size on the course of the aforementioned erosion stages must be considered.

For a comprehensive understanding of erosion, research in this area focuses on analyzing these factors through multiple technological approaches with the aim of gaining a deeper understanding of erosion development mechanisms. The modulation of a continuous jet to induce discontinuity in the water flow, resulting in discrete pulses acting on the material surface, can be generated by various methods. Foldyna introduced the ultrasonically excited pulsating water jet (PWJ) technique [Foldyna 2005]. Although the PWJ was developed for the disintegration of hard-to-cut materials, its application has been extended and intensively examined in other applications such as water jet erosion prediction or surface treatment of metals [Foldyna 2012], [Klich 2017], [Svabenska 2020]. The cited studies highlight the importance of grain boundaries for

erosion development in the erosion incubation stage of metallic materials. This creates a knowledge gap in understanding the effect of grain size on erosion progression.

Therefore, this work focuses on the effects of material hardness and grain size on hydrodynamic erosion resistance. In this paper, samples of pure copper that were subjected to vacuum heat treatment to modify the resulting grain size. Samples with a polished surface were subjected to PWJ erosion at single line passes with varying feed rates of 0.5 - 4 mm/s. Different erosion characteristics of erosion depth and removed volume are expected to be observed at varying feed rates, along with the change in hardness and grain size.

## 2 MATERIALS AND METHODS

### 2.1 *Materials and preparation*

The material under investigation was technically pure copper. To achieve recrystallization of the initial state (***INS***) with a small grain size into a material with larger grains, two different heat treatments (***HT***) were applied, providing three material states with varying grain sizes. Conditions of ***HT*** were selected based on the thermal stability study performed in [Zhang 2022], where it was reported that the recrystallization nucleation starts at approximately 400°C, and an increase in annealing temperature up to 1000°C results in complete recrystallization followed by grain coarsening. The ***HT*** of specimens with dimensions of 5x25x100 mm was carried out in a vacuum furnace, i.e., the surface of the samples during the ***HT*** was not oxidized due to the high-temperature exposure. Specimens were processed with the following conditions: 600°C/1h (labeled as ***HT1***) and 900°C/1h (***HT2***).

Surface of specimens was prepared by usual metallographic procedures (mechanical grinding and polishing). The electrolytic polishing at 12 V was the final step. The electrolyte had a temperature of 12 °C and consisted of distilled water, phosphoric acid, ethanol, and propanol. To reveal the microstructure of samples for SEM analysis, chemical etching was performed using nitric acid solution in water.

Hardness analysis using a DuraScan 70 G5 ZwickRoell hardness tester (Vickers method) was performed with a minimum of 5 indents for each material condition.

A general assessment of erosion grooves formed by PWJ application for all material states was performed using an Olympus DSX1000 optical microscope. Microstructure and more detailed fractographic studies, i.e., observations of the morphology and shape of the erosion damage, were conducted using a Tescan Lyra 3 XMH FEG/SEMxFIB scanning electron microscope (SEM). The SEM micrographs in ***Fig. 1a*** confirmed a homogeneous microstructure in all material states under investigation. Small particles consisting of copper and oxide were observed, similar to those reported in [McQueen 1986]. The EBSD detector built into the SEM was used, and AZtec Oxford software was employed to determine the crystallographic orientation and the material grain size. The depth and volumetric mass removal at the disintegrated surface of erosion grooves were evaluated by the Alicona InfiniteFocus G5 focus variation-based measuring system.

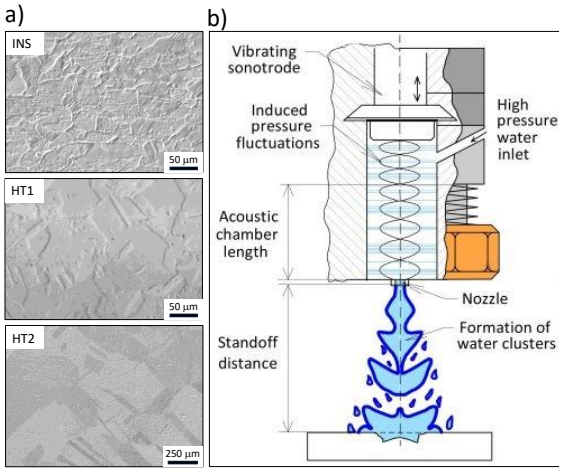


**Figure 1:** a) SEM micrographs of the microstructure of copper in all three material states: Initial (INS), heat-treated 600°C/1h (HT1), and heat-treated 900°C/1h (HT2), b) principle of PWJ.

To process the EBSD data, Kernel Average Misorientation (KAM) analysis was employed. Average lattice disorientation inside the grains was evaluated based on local lattice deformations induced by dislocation density after plastic deformation. The misorientation angle was set to 5°.

### 2.2 *PWJ treatment*

The specimens were subjected to the influence of an ultrasonically driven PWJ. The principle of PWJ is shown in ***Fig. 1b***. The Hammelmann HDP 253 hydraulic pump was used to supply high-pressure water to the acoustic chamber. An optimum acoustic chamber length was adjusted according to Nag [Nag 2019]. The effective standoff distance (SOD), i.e., optimum distance between the nozzle and the material surface, was assessed using a stair trajectory [Hloch 2020]. An acoustic generator was adopted to create the high-frequency pulses of the sonotrode. Due to the pressure pulses created, the continuous water jet was disintegrated into clusters of individual water droplets at a certain distance from the nozzle orifice (see ***Fig. 1b***). The PWJ was applied with a linear trajectory of jet movement. Two sets of parameters based on supply pressure, as listed in ***Table 1***, were used to create erosion grooves, and three repetitions were applied to increase the statistical relevance of measurements. The pressure used in the experiments was chosen to be 20 and 30 MPa, which allowed for monitoring the erosion zones from incubation to the advanced erosion stages. This setting is essential for the ability to qualify and compare possible different mechanisms of erosion development between the material states. At the used frequency of 40 kHz and nozzle diameter of 0.6 mm, the optimal parameters of the acoustic chamber length were set to 8 and 10 mm for 20 and 30 MPa, based on the methodology presented by [Nag 2019], at which the acoustic assembly converts the electrical signal into mechanical movement most efficiently.

**Table 1** Technological parameters of waterjet treatment

| **Supply pressure** | **Sonotrode frequency** | **Nozzle diameter** | **Chamber length** |
|---|---|---|---|
| 20 MPa<br>30 MPa | 40 kHz | 0.6 mm | 8 mm<br>10 mm |
| **Jet speed** | **Volumetric flow rate** | **Standoff distance** | **Feed rate** |
| 180 m/s<br>220 m/s | 3.06 l/min<br>3.74 l/min | 23 mm<br>35 mm | 0.5 – 4 mm/s |

The incrementally increasing feed rate of the water jet was adopted for this study. Concerning the frequency of 40 kHz, it is possible to recalculate the feed rate to the number of impacts per unit of length (0.5, 0.67, 1, 1.3, 2, and 4 mm/s feed rate corresponds to the number of impacts ranging from 80,000 to 10,000). Tuning of the feed rate ensured that both the initiation and advanced stages of erosion were reached (see ***Fig. 2***).

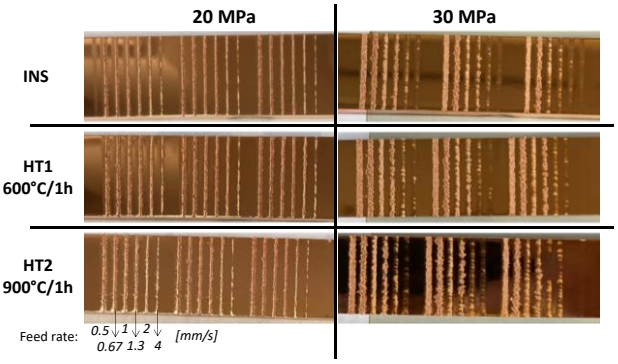


**Figure 2:** Erosion grooves created by PWJ under two supply pressures.

## 3 RESULTS AND DISCUSSION

### 3.1 *Grain size, misorientation angle, texture, and hardness*

EBSD analysis was used to characterize the experimental material before and after heat treatment and assess the effect of exposure to PWJ under two pressure conditions. The metallographic cuts were prepared with two orientations to the rolling direction (transversal and longitudinal). All material states exhibited fairly equiaxed grains in both orientations, containing a high frequency of annealing twins, i.e., special grain boundaries. The fraction of Σ3 boundaries was 28, 55, and 72%, respectively, for material states ***INS***, ***HT1***, and ***HT2***. It corresponds to Zhang [Zhang 2022], where a higher number of annealing twins in the microstructure was reported for the higher temperature of heat treatment. Multiple twinning or twin chains observed in the work of Afifeh [Afifeh 2021] have not occurred in the current study. According to the results of [Cayron 2011], in the case of materials with a low to medium stacking fault energy, such as copper, the early stages of grain growth at recrystallization are accompanied by a polysynthetic or lamellar twin. This twinning type, with more than two parts in one grain, occurred in the current study. Evaluation of the grain size was performed with the inclusion of special boundaries. The combination of temperature and time exposure during heat treatment resulted in a uniform recrystallized microstructure with a homogeneous grain size distribution. The average grain size listed in ***Table 2*** shows the coarsening of approximately 1.6x for an HT temperature of 600°C and 7.2x for 900°C. These results correspond to the work of Zhang [Zhang 2022], where an increase in grain size by a factor of 10 times higher due to annealing at 1000°C/1h from the initial state with a grain size of 16 µm was reported.

**Table 2:** Material characteristics

| Label | Material state | Grain size considering twins | Hardness HV0.5 |
|---|---|---|---|
| ***INS*** | initial | Average: 53 µm | 97.0±1.8 |
| ***HT1*** | 600°C/1h | Average: 84 µm | 39.2±0.7 |
| ***HT2*** | 900°C/1h | Average: 380 µm | 35.9±2.2 |

Plastic deformation stored in the grains can be determined by KAM analysis, where the KAM parameter describes the local lattice deformations induced by dislocations. The increased dislocation density results in a higher value of the KAM parameter [Poloprudsky 2024]. It represents the state when more geometrically necessary dislocations were produced to accommodate the strain gradient of the neighboring grains [Ren 2023]. In the present work, KAM analysis, performed before the PWJ application, was used to assess the degree of plastic deformation stored in sample surfaces of all material states (***INS***, ***HT1***, and ***HT2***). ***INS*** state exhibits some degree of plastic deformation, expressed as a misorientation angle of approximately 2.5° in most grains of the material. It is related to the rolling production of copper sheets. The plastic deformation related to dislocation density was distributed homogeneously, contrary to the paper of Atefi [Atefi 2022], where misorientation was concentrated near grain boundaries, and small grains and large grains showed less misorientation. Annealed states (***HT1*** and ***HT2***) revealed that recrystallization occurred and, except for grain coarsening, also removal of the deformed structure from rolling was observed (misorientation angle was close to 0°) (see ***Fig. 3a***). EBSD analysis also provided data on the texture of the material (i.e., the directed orientation of the grains or their preferential stretching) introduced into the microstructure during plastic deformation. The results for the material states before PWJ treatment are in ***Fig. 3b***. The ***INS*** state exhibited the preferred orientation of grains in the [111] direction, corresponding to a multiple of uniform distribution value (MUD) of approx. 3.3, and then partially in [001] direction. The annealed states (***HT1*** and ***HT2***) underwent recrystallization, where the texture was removed or rearranged. The ***HT1*** state is almost without texture. It is expressed in the stereographic triangle by a nearly homogeneous green color corresponding to a MUD value of approximately 1. The ***HT2*** state consists of grains with slightly preferred orientation in the [001] direction.

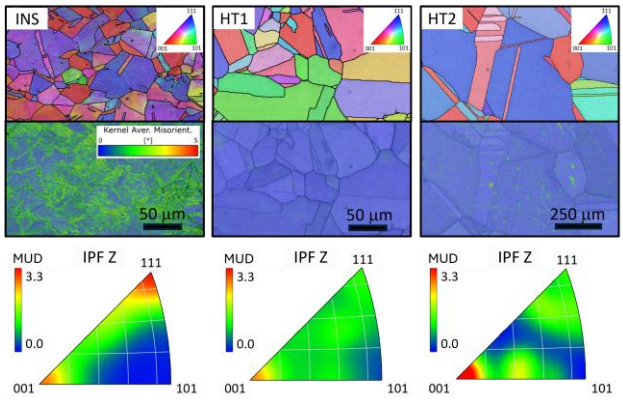


**Figure 3:** a) KAM analysis maps before PWJ treatment, b) Inverse Pole Figures (IPF) in Z axis for texture analysis.

The hardness values based on the Vickers method (HV0.5, see ***Table 2***) were measured on metallographic samples for all material states (***INS***, ***HT1***, ***HT2***) before applying PWJ. The ***HT1*** and ***HT2*** states show a significantly lower hardness (approximately 2x) than the ***INS*** (rolled) state. The ***INS*** state exhibits the highest HV value due to the smallest grain size and the plastic deformation introduced into the material during sheet metal production by rolling. Softening due to HT (***HT1*** and ***HT2***) corresponds to a fully recrystallized state with a larger grain size. Similar results were presented in the work of Ren [Ren 2023], where the decrease in hardness was accompanied by an increase in ductility in dependence on the increase in grain size by heat treatment at 900°C.

### 3.2 *Observation of erosion morphology*

***Fig. 4*** shows an overview of erosion grooves obtained using the PWJ with a supply pressure of 30 and 20 MPa for three material states (***INS***, ***HT1***, and ***HT2***) and six levels of feed rate.

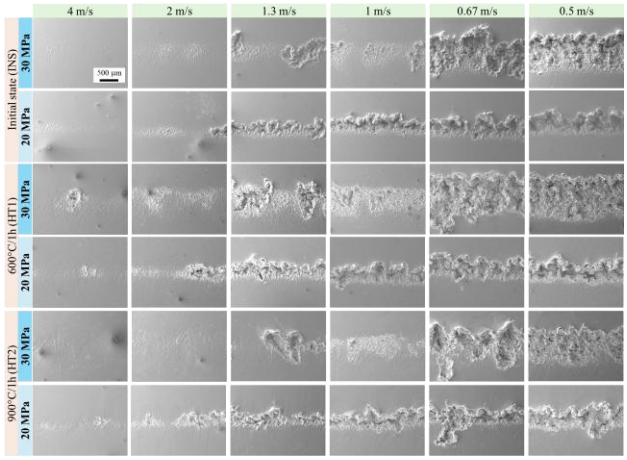


**Figure 4:** Overview of erosion grooves on copper in three material states, created by supply pressure of 20 and 30 MPa and all levels of feed rate.

The typical morphology of erosion traces created in the present work on copper samples corresponds to the results observed also on other types of material, such as aluminum alloy [Poloprudsky 2022], brass [Lehocká 2018], or austenitic steel [Srivastava 2020].

The feed rate was selected as a primary PWJ parameter to control the impact distribution. The higher feed rate results in shorter exposure to the action of water droplets, i.e., in a smaller number of impacts per unit of length. It is also related to the shallower and narrower grooves. High feed rates (the maximum used in this work was 4 mm/s) result in surface roughening and signs of material removal. It can be assumed that further increasing the feed rate could lead to a complete limitation of material loss, and only an incubation period of erosion would occur. With the decrease in feed rate, the number of water clusters hitting the surface increases, and the erosion grooves become more developed. According to Poloprudský [Poloprudsky 2024b], a similar effect of feed rate was observed for PWJ with constant frequency moving on a linear trajectory. Further reduction of the feed rate (less than 0.5 mm/s used in this study) would lead to a stabilization of the roughness of the eroded groove bottom, as also described in [Hloch 2024]. The material removal rate would also be gradually reduced and slowed down, as a result of inducing advanced erosion phases defined as “depletion” [Hloch 2020].

The supply pressure of 30 MPa creates wider erosion grooves than that of 20 MPa. Nevertheless, a certain inhomogeneity of erosive effects was observed, manifesting in alternating sections with roughened and eroded surfaces or instability of erosion grooves' width, visible not only in the overview of SEM images in ***Fig. 4*** but also in ***Fig. 2*** obtained by a standard camera. The inhomogeneity of the groove shape along a linear trajectory occurred independently of the material state. It can be attributed to several factors, including the sonotrode frequency. In the work of Stolarik [Stolarik 2023], it is described that the generated frequency of the sonotrode can deviate during the experiment, affecting the volume of water clusters. In the present case, the optimum values of SOD and frequency were applied, i.e., the higher groove shape irregularity for 30 MPa supply pressure can be explained by higher pressure fluctuations of PWJ inside the acoustic chamber.

The well-developed erosion groove consists of a deep valley surrounded by two borders. The detailed analysis of erosion features found in erosion grooves and their vicinity was performed. Examples of the most typical attributes are in ***Fig.5***. The first feature that must be mentioned is the different morphology of the opposite borders of the erosion groove. Edges bordering an erosion groove and mainly the transition region between the groove bottom and the not-eroded material in the groove vicinity were found to be slightly different on each side. The inhomogeneity on both sides is predominantly in the form of varying heights or volumes of material upheaval. The discrepancy in upheaval formation is visible in ***Fig. 5a***, where the erosion groove has a linear footprint due to a jet head moving linearly with constant velocity (a certain value of feed rate). This discrepancy can be observed not only in the case of linear erosion footprints (see ***Fig. 5a***) but also in the case of a similar experiment [Poloprudsky 2024] where the stationary position of the jetting head at the defined time created erosion crater, which is in the form of a dot, and usually exhibits a crescent or arc-shaped form (see ***Fig. 5b***). The exposure time in the case of stationary action of the water jet has an analogous role as the feed rate in the present experiment. This irregularity, visible in ***Fig. 5*** for both cases, can be attributed to a non-homogeneous velocity field in the nozzle, as described in the work of Hong [Hong 2023]. As presented in ***Fig. 5***, one side of a groove or a dot is typically characterized by a dominant pile-up of material (see the upper part of ***Fig. 5***), while the opposite border usually has a more fluent transition (see the lower part of ***Fig. 5***).

The creation of the pile-up is related to the action of the lateral jet and starts as soon as the depth of the erosion groove/crater is bigger than the size of the impinging water droplets. Behind the dominant pile-up, there is usually a smooth surface without roughening, because the upheaved material forms a barrier shielding the vicinity of the groove from the impact of stray water drops. Nevertheless, in this area, a specific feature, which can be described as a chimney vent, can be observed. It is an exit of a created micro-tunnel due to lateral jetting (see ***Fig. 5***). Surprisingly, the vents can be found at quite remote distances (depending on conditions such as plasticity of material, depth of erosion groove, and level of water pressure). The complexity of subsurface microchannels was observed in the work of Hloch [Hloch 2022].

The groove border, which is opposite to the pile-up site (see the lower part of ***Fig. 5***), has a less sharp transition, usually without pile-up; it is rather a smooth transition from the heavily eroded surface, a roughened area, through a slightly deformed area, up to a not-deformed area. Inside the roughened and deformed areas, it is possible to observe surface ripples as signs of plastic deformation. These features, which are dominant in the initial stages of erosion (preincubation and incubation), are driven by exposing the microstructural parts, such as grain or twin boundaries, to both the direct water droplet impingement and the action of lateral flow. Certain materials [Poloprudsky 2021] exhibit the creation of mechanical twins at a small distance from the pile-up, i.e., twins whose formation is related to a repetitive action of clusters of water droplets impinging mechanically the material surface. In the present case of copper with various grain sizes due to heat treatment, all the material states contained annealing twins in the microstructure. The formation of surface steps inside the grains was already observed [Poloprudsky 2024b]. A comparable situation occurred in the present case, where the area of the roughened and mildly deformed surface

was relatively flat and filled by enhanced grain and twin boundaries, highlighted by very mild material upheaval.

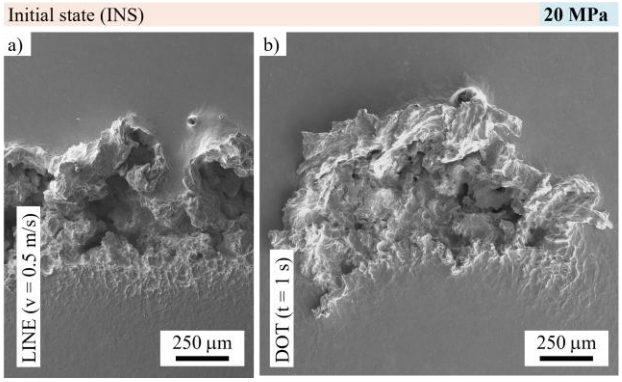


**Figure 5:** Comparison of a) erosion groove in the form of LINE for jetting for low feed rate, b) erosion pit in the form of DOT for stationary jetting.

A detailed view of common fractographic features observable independently of the material state is in ***Fig. 6***.

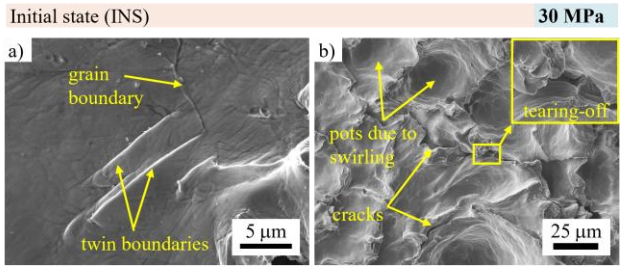


**Figure 6:** Details of fractographic features: a) enhancement of grain and twin boundaries, b) rounded pits from swirling, cracks, and freshly torn-off area.

The enhanced grain and twin boundaries are shown in ***Fig. 6a***. ***Fig. 6b*** presents a detail of the bottom of the erosion groove formed mainly from deep valleys and sharp peaks. They can, due to the action of the water jet hitting the peaks and circulating in the valleys, blunt the sharp edges. Usually, at the bottom of valleys, it is possible to observe cracks as the beginning of material undercutting and material removal. Occasionally, it is possible to find signs of fresh fracture after tearing off the part of the material just before this area is smoothened and blunted by water flow, and possibly with the abrasive assistance of eroded metallic parts. The presence of the rounded pits suggests water swirling. It can be supposed that it happens due to a mechanism like in natural conditions in rivers where pot-holes are created due to swirling of water and abrasive action of smaller stones, i.e., eroded parts of rock [Ji 2018].

### *3.3 Quantitative analysis of material erosion*

Profiles of erosion grooves and the material volume removed by erosion were evaluated using optical microscopy with focus variation. The results of this analysis showed that the measurable material loss, as evaluated by the removed volume or depth of erosion, is too low for their quantitative evaluation at feed rates of 1 – 4 mm/s. At these feed rates, measurable material removal occurred only in stochastically distributed areas along the PWJ movement path, while in some regions, only material roughening was observed. Therefore, due to the inconsistency of the achieved erosion efficiency, these feed rates were identified as inadequate for quantitative analysis of volume loss or depth. The two lowest feed rates of 0.5 and 0.67 mm/s showed evenly distributed erosion across the entire path of PWJ movement; therefore, these speeds were used for further material loss analysis.

The volume removed by the action of PWJ from the measured length of 10 mm of the erosion groove is plotted in ***Fig. 7***. The results showed that the largest removed volume was at a pressure of 30 MPa using a feed rate of 0.67 mm/s. A typical PWJ erosion trend in literature indicates that as the feed rate increases, the number of impacts of water segments on the material reduces, resulting in a reduction of the induced erosion [Stolarik 2024]. However, in our case, the trend is opposite for all used material states when comparing 0.5 and 0.67 mm/s feed rate for $p$ = 30 MPa. A possible explanation for the absence of a specific trend across all the tested materials could be that the induced impact pressure $p_i$ at a supply pressure of 30 MPa significantly exceeds the yield strength of the material, regardless of its material state obtained by heat treatment. For the acceleration phase of erosion, according to Kamkar [Kamkar 2013], a stochastic and rapid material removal in the form of small fragments is typical.

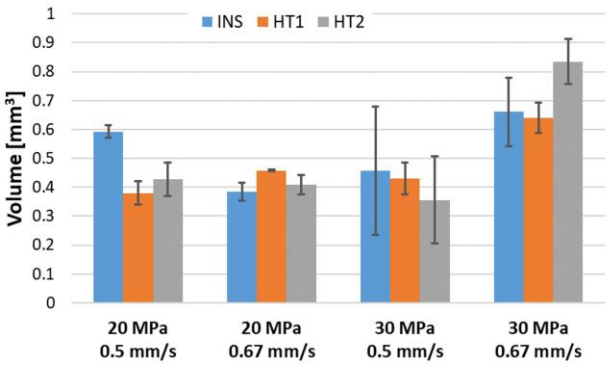


**Figure 7**: Volume of removed material in dependence on feed rate for two supply pressures, and the INS, HT1, and HT2 material states.

Increasing the impact density per unit length to 80,000 imp/mm (feed rate of 0.5 mm/s) led to denser droplet distribution, which resulted in a decrease in the time available for the development of comprehensive impact pressure and the subsequent phase with intensive lateral flow, which significantly affects the rate and speed of erosion [Huang 2018]. At this frequency, individual segments impacted at a distance of *Wsi* = 13 nm from each other (***Fig. 8a***). Thus, the erosion effect at lower feed rates may be less pronounced compared to higher feed rates, where, conversely, the reduced impact density per unit length of 59 701 imp/mm (feed rate of 0.67 mm/s) resulted in more favorable conditions for the development of individual interaction phases between water segments and the material surface. In this case, the impact distance between individual segments also increased to *Wsi* = 18 nm (***Fig. 8b***). The imperfect interaction at an extremely low feedrate is caused by subsequent impacts being spatially and temporally close to each other. The impact may be dampened by a water layer caused by a previous impact and disturbed by the following impact. While an increment of feed rate doesn't completely remove these effects, it alleviates them, depending on the selected feed rate.

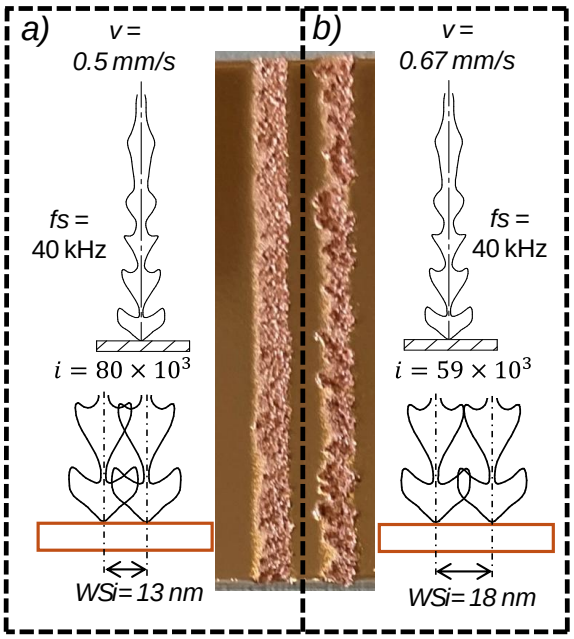


**Figure 8:** Comparison the distance between water segment impacts at a feed rate a) 0.5 mm/s and b) 0.67 mm/s

Interestingly, when comparing the volume of removed material depending on the heat treatment, i.e., for ***INS***, ***HT1***, and ***HT2*** states, at a feed rate of 0.5 mm/s, a decrease in the removed material is also observed with a decrease in hardness (***INS***, ***HT1***, ***HT2***), particularly for $p$ = 30 MPa. This observation can be attributed to the fact that the HT process, in addition to altering the hardness, also changes the average grain size and plasticity, which were increased with the intensity of HT. In the study of Poloprudský [Poloprudsky 2024], it was observed that the incubation stages of erosion are visible at the grain boundaries through their exposure. Furthermore, with the increase in their load, cracks are formed, leading to the initial removal of material. Therefore, an increase in grain size at ***HT2*** and ***HT1*** resulted in a decrease in the amount of grain boundaries, leading to better material resistance and less material loss compared to the ***INS*** state. Furthermore, the restored plasticity of the material after HT led to an increase in the amount of energy that the material could absorb. However, at a speed of 0.67 mm/s, an opposite trend was observed with increasing material volume loss, together with the intensity of HT. This result could be attributed to the better-developed interaction between the jet and the material, attributable to an extended distance between consecutive impacts. This extended distance potentially results in a longer duration of impact pressure, thereby making the material's hardness the predominant factor. Therefore, it can be stated that in 30 MPa:

- **plasticity** and **grain size** are significant parameters at lower feed rates, where imperfect development of segment impact phases occurs. With HT intensity, the plasticity of the material improves, and grain size increases, making the material more resistant to erosion,

- higher feed rates create favorable conditions for the development of each impact segment, creating better conditions for **hardness** to play a significant role. Furthermore, with increased HT intensity, hardness diminishes, which subsequently results in an increase in the material removal rate.

When comparing the results for 30 MPa with those for 20 MPa, in the case of lower supply pressure, a variable loss of material volume was observed, with no dominant trend related to the effect of heat treatment at both feed rates of 0.5 and 0.67 mm/s. The following two hypotheses were formed to explain the observed behaviors:

First, the reduction in supply pressure and therefore in impact pressure could be related to the creation of erosion during the initial impacts of water clusters on the surface. However, with increasing exposure time, the bottom of the groove could be flooded, and therefore, the impact of another liquid in the form of water clusters on the created water film causes the breakdown of the impact pressure, similar to what is described by Fujisawa [Fujisawa 2019]. It results in a situation where the impact pressure causes the compression of the liquid film, which results in the generation of two shock waves travelling downwards in the liquid film. This may lead to a reduction in erosion potential, accompanied by irregular material removal.

Second, the pressure changes may also be the effect of the PWJ technological device. The lower operating pressure is achieved by reducing the rotations of the hydraulic pump. This may have a significant effect on the frequency of pressure fluctuations in the high-pressure pipe that transports water from the pump to the acoustic chamber. In the acoustic chamber, the pump fluctuations could interact with the pressure waves generated by the sonotrode. This can lead to their merging or mutual negation, which also causes different characteristics of the fluctuating pressure passing through the water nozzle, and therefore the generated water segments. Therefore, at this pressure, erosion is more irregular and unpredictable due to technological conditions, suppressing the effect of heat treatment on the removed material volume.

These two main hypotheses mentioned, nevertheless, need to be more intensively investigated. The irregular material loss at the lower pressure of 20 MPa is interesting and worth investigating it further. Potential cause considers groove flooding and breakdown of the impact pressure, it creates a condition analogous to submerged or partially submerged jetting. This phenomenon was studied in the work of Hloch or Stolárik on steels [Hloch 2024b], [Stolarik 2024].

Dispersion of water clusters and irregular material loss can lead to a significant increase in error bars in the measurement of the removed volume. It can be observed that the dispersion of the measured values increases at 30 MPa (max. 48.6%), which may be related to the more intense wave interaction (merging or interference of pressure waves) in the acoustic chamber, leading to their instability and fragmentation. At 20 MPa, the error bars are relatively small (max. 13.3%), which indicates that the observed deviations cannot be attributed primarily to the inhomogeneity of the material, but rather to the technological factors of the PWJ and the nature of the generated stream. From a practical point of view, this means that in future experiments, it is necessary to verify this dispersion hypothesis and separate the error rate caused by technological problems.

The variation of the generated average depth of the erosion groove measured at 10 mm of the erosion length is shown in ***Fig. 9***. The trends observed with 30 MPa support the trends of the removed volume described above. It is also possible to observe the irregular trends of the average depth observed at 20 MPa, similar to the removed volume. This indicates heterogeneous material removal, where the aforementioned fluctuations in the acoustic chamber caused the generation of water clusters with different properties, consequently showing a different erosion response within one transition cycle (line). At the same time, the PWJ device automatically adjusts the actual generated frequency [Nag 2019] according to the

resistance in the acoustic chamber. Induced fluctuations from the high-pressure water supply could be reflected from the walls of the acoustic chamber towards the sonotrode. This resulted in variations in the resistance of sonotrode oscillation, as the PWJ technological device constantly tried to attain resonance by adjusting the actual generated frequency. This may also result in the formation of water clusters with varying volumes within a single passage, thereby producing different erosion potentials. This leads to inhomogeneity of erosion and the creation of a stochastic distribution and uneven bottom of the erosion groove, which is reflected in the measurement of the average depth.

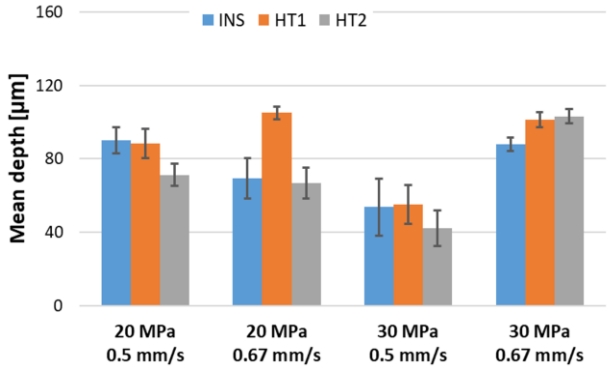


**Figure 9:** Depth profiles in dependence on feed rate for two supply pressures of 20 and 30 MPa, and the INS, HT1, and HT2 material states.

For the profile analysis of the eroded groove, graphical representations of cross-sections were created at five locations along the erosion line (***Fig. 10***). From these cross-sections, it is visible that at each groove location, the groove bottom is different without any signs of continuity. This confirms the inhomogeneous removal of material characterised by the peeling of the fragments and the formation of a stochastic structure at the bottom of the erosion groove, similar to the one observed in [Hloch 2022]. This inhomogeneous removal may also depend on local material properties, more precisely, the distribution and orientation of surrounding grains at the point of impact of the water segment. However, in each case, it is possible to observe plastic deformation of one side of the erosion trace (see right part of profiles in ***Fig. 10***), where the material was extruded above the level of the original polished surface, as also observed in the prior SEM images (***Fig. 5a***). Such behavior was also observed in the work of Hloch [Hloch 2022], as a clear evidence of the influence of lateral flow and the plasticity of the material during the erosion process. Interestingly, the material extrusion always occurred only in the right part of the erosion groove. This indicates an inhomogeneous influence of the lateral flow in the groove. This phenomenon may be caused by technological problems associated with the decentered trajectory of the generated water clusters, which leads to an uneven distribution of the load after impact and to a different lateral flow in the impact cross-section. Such asymmetry may arise due to several factors, such as nozzle wear (wear to a cylindrical shape), insufficiently adjusted perpendicularity of the nozzle to the target surface, or water supply entry to the acoustic chamber from only one side, which leads to an uneven distribution of energy in the cluster cross-section. Solving these problems could lead to the generation of a potentially perpendicular water stream with an evenly distributed energy of the water cluster.

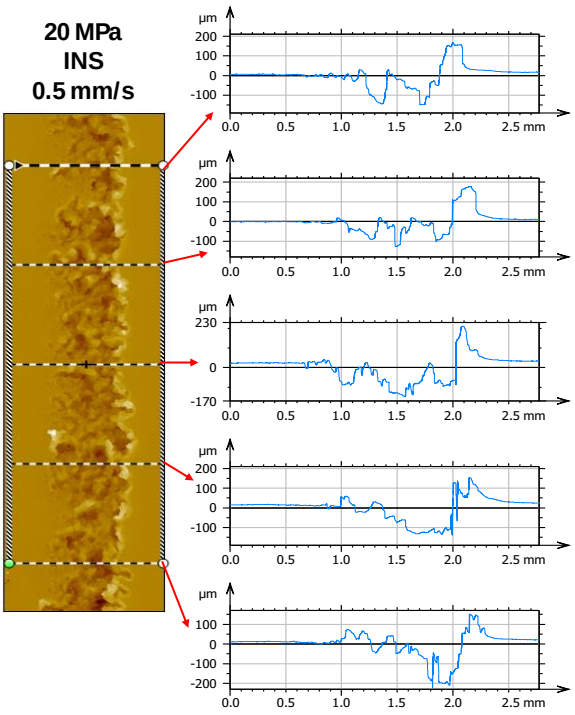


**Figure 10:** Analysis of the erosion groove geometry profile after PWJ line transition

The solution for how to improve the homogeneity of the eroded/modified surface, even with a potentially unstable erosion conditions, could be in future research and applications reached under certain conditions by increasing the number of passes over the sample in the same line, which could lead to a stabilization of erosion distribution [Stolárik 2025]. It could subsequently allow a more precise observation of the influence of material properties on the induced erosion. Another way could be to use flat nozzles that offer a distribution of impact energy over a larger area, leading to the creation of a more homogeneous groove bottom observed in [Lehocká 2016].

The hypothesis, that "smaller grain sizes resist hydrodynamic erosion better than larger ones", was studied in the work of Reddy [Reddy 1987], where some materials do not conform to this hypothesis. The similar hypothesis of our work for copper with variable grain size impacted by PWJ was not sufficiently proven as well. Actually, more complex dependencies were observed than only the grain size effect, because it is related to a change in the hardness as well as the feed rate dependence.

In the present work, even a 7 times smaller grain size observed in the ***INS*** sample (53 µm) compared to the highest grain size for ***HT2*** (380 µm) had conclusive monotonous effect on the erosion depth of the samples, even when it is accompanied by a significant hardness changes (decrease in hardness from HV = 97 for the ***INS*** state to HV = 35.9 for the ***HT2*** state, i.e., 37% of the initial state). The hardness values of the heat-treated samples compared to the initial state were halved; nevertheless, the changes in eroded depth don't show a monotonic trend with heat treatment, but rather complex behavior influenced by feedrate. It can be attributed to reaching the maximum values, i.e., the saturation level. It indicates the jet's hydraulic power overpowers the material strength thresholds. Regardless of changes in microstructure and hardness due to the heat treatment process, the conditions of PWJ treatment led to repetitive impact pressure, nearly 239.52 MPa, overcoming the mechanical properties or reaching their limits.

The changes described in microstructural features and mechanical properties nevertheless did not affect the erosion capability of the PWJ within the selected range of input conditions. Much lower input conditions of PWJ probably need to be chosen to observe the effect of the heat treatment process on erosion resistance.

## 4 CONCLUSIONS

This study introduced a pulsating water jet to examine the effect of grain size on erosion resistance. Samples of pure copper exhibiting three variants of material states (grain sizes) due to heat treatment were treated using a PWJ with a linear trajectory of the jet and increasing feed rate. From the results of the research, the following conclusion can be drawn:

- EBSD and KAM analysis proved that recrystallization of copper was reached by adopting two types of heat treatment (600°C/1h, 900°C/1h), accompanied by the removal of texture and plastic deformation from sheet rolling in the initial state.

- At a feed rate of 0.5 mm/s, owing to the imperfect interaction between the discrete water clusters and the material, an increase in the HT intensity subsequently enhanced the plasticity of the grains, resulting in improved erosion resistance as demonstrated by the depth and removed volume.

- At a feed rate of 0.67 mm/s, the hardness determining the erosion response decreased as the HT intensity increased, thereby subsequently reducing the material's erosion resistance.

- The results showed that the maximum material removal and the greatest depth were achieved at 30 MPa and 0.67 mm/s due to sufficient time to develop sufficient impact pressure intensity.

- SEM observations showed an irregular shape of the generated grooves. These irregularities were observed for all the tested samples and can be attributed to both the inhomogeneity of the material and, to some extent, to the transmission of ultrasonic signals into the hydraulic system within the sonotrode.


## ACKNOWLEDGMENTS

The financial support was provided by the Slovak Research and Development Agency under project contract No. APVV-22-0391. The authors are grateful for the execution of the experiments at the Institute of Geonics of the Czech Academy of Sciences, Ostrava–Poruba, Czech Republic, namely to Dr. Josef Foldyna, for the opportunity to perform the experiments using Pulsating Water Jet Technology. The presented work was also supported by a project for the long-term conceptual development of the research institution RVO: 68145535.


## REFERENCES


[Afifeh 2021] Afifeh, M., et al. Effect of post-annealing on the microstructure and mechanical properties of nanostructured copper. Materials Science and Engineering: A, 2021, Vol.802, 140666. https://doi.org/10.1016/j.msea.2020.140666

[Ahmad 2009] Ahmad, M., et al. Experimental assessment of droplet impact erosion resistance of steam turbine blade materials. Wear, 2009, Vol.267, No.9-10, pp 1605-1618. https://doi.org/10.1016/j.wear.2009.06.012

[Atefi 2022] Atefi, S., et al. A study on microstructure development and mechanical properties of pure copper subjected to severe plastic deformation by the ECAP-Conform process. Journal of Materials Research and Technology, 2022, Vol21, pp 1614-1629. https://doi.org/10.1016/j.jmrt.2022.09.103

[Bowden 1958] Bowden, F.P., et al. Damage to solids by liquid impact at supersonic speeds. Nature, 1958, Vol.181, pp 873–875. https://doi.org/10.1038/181873a0

[Cayron 2011] Cayron, C. Quantification of multiple twinning in face centred cubic materials. Acta Materialia, 2011, Vol.59, No.1, pp 252-262. https://doi.org/10.1016/j.actamat.2010.09.029

[Chlupova 2023] Chlupova, A., et al. Effect of pulsating water jet processing on erosion grooves and microstructure in the subsurface layer of 25CrMo4 (EA4T) steel. Wear, 2023, Vol524, 204774. https://doi.org/10.1016/j.wear.2023.204774

[Choi 2015] Choi, D.H., et al. Long-term investigation of erosion behaviors on metal surfaces by impingement of liquid droplet with high-speed. Journal of Mechanical Science and Technology, 2015, Vol29, pp 1085–1091. https://doi.org/10.1007/s12206-015-0220-0

[Cook 1928] Cook, S.S. Erosion by water-hammer. Proceedings of the Royal Society of London. Series A, Containing Papers of a Mathematical and Physical Character, 1928, Vol.119, No.783, pp 481–488. https://doi.org/10.1098/rspa.1928.0107

[Foldyna 2005] Foldyna, J., et al. Rock cutting by pulsing water jets. In: ISRM EUROCK. ISRM, Czech Republic 2005. ISRM-EUROCK-2005-021.

[Foldyna 2012] Foldyna, J., et al. Erosion of Metals by Pulsating Water Jet. Tehnicki Vjesnik - Technical Gazette, 2012, Vol.19, No.2, pp 381-386. ISSN 1330-3651.

[Fujisawa 2022] Fujisawa, K. Simulation of lateral jet formation in high-speed liquid droplet impingement and its impact on crater side wall. Annals of Nuclear Energy, 2022, Vol.175, 109202. https://doi.org/10.1016/j.anucene.2022.109202

[Fujisawa 2023] Fujisawa, K. On erosion transition from the incubation stage to the accumulation stage in liquid impingement erosion. Wear, 2023, Vol.528, 204952. https://doi.org/10.1016/j.wear.2023.204952

[Fujisawa 2019] Fujisawa, K., et al. Influence of surface roughness on liquid droplet impingement erosion. Wear, 2019, Vol.432, 202955. https://doi.org/10.1016/j.wear.2019.202955

[Huang 2018] Huang, F., et al. Study on lateral jetting range during an arc-curved jet impacting nonplanar solid surfaces. Journal of Fluids Engineering, 2018, Vol.140, No.10, 101201. https://doi.org/10.1115/1.4039945

[Haller 2002] Haller, K.K., et al. Computational study of high-speed liquid droplet impact. Journal of Applied Physics, 2002, Vol.92, pp 2821-2828. https://doi.org/10.1063/1.1495533

[Haller 2003] Haller, K.K., et al. Shock wave formation in droplet impact on a rigid surface: Lateral liquid motion and multiple wave structure in the contact line region. Journal of Fluid Mechanics, 2003, Vol.490, pp 1-14. https://doi.org/10.1017/S0022112003005093

[Hloch 2020] Hloch, S., et al. Effect of pressure of pulsating water jet moving along stair trajectory on erosion

depth, surface morphology and microhardness. Wear, 2020, Vol.452, 203278. https://doi.org/10.1016/j.wear.2020.203278

[Hloch 2022] Hloch, S., et al. Subsurface microtunneling in ductile material caused by multiple droplet impingement at subsonic speeds. Wear, 2022, Vol.490, 204176. https://doi.org/10.1016/j.wear.2021.204176

[Hloch 2024] Hloch, S., et al. Erosion development in AISI 316L stainless steel under pulsating water jet treatment. Engineering Science and Technology, an International Journal, 2024, Vol.50, 101630. https://doi.org/10.1016/j.jestch.2024.101630

[Hloch 2024b] Hloch, S., et al. Submerged pulsating water jet erosion of ductile material. Wear, 2024, Vol.538, 205243. https://doi.org/10.1016/j.wear.2024.205243

[Hong 2023] Hong, S., et al. Investigation on the erosion characteristics of liquid–solid two-phase flow in tee pipes based on CFD-DEM. Journal of Marine Science and Engineering, 2023 Vol.11, 2231. https://doi.org/10.3390/jmse11122231

[Ji 2018] Ji, S., et al. The relationship between diameter and depth of potholes eroded by running water. Journal of Rock Mechanics and Geotechnical Engineering, 2018, Vol.10, No.5, pp 818-831. https://doi.org/10.1016/j.jrmge.2018.05.002

[Kamkar 2013] Kamkar, N, et al. Water droplet erosion mechanisms in rolled Ti–6Al–4V. Wear, 2013, Vol.301, No.1-2, pp 442-448. https://doi.org/10.1016/j.wear.2013.01.005

[Kirols 2015] Kirols, H.S., et al. The effect of initial surface roughness on water droplet erosion behaviour. Wear, 2015, Vol.342, pp 198-209. https://doi.org/10.1016/j.wear.2015.08.019

[Klich 2017] Klich, J., et al. Influence of variously modified surface of aluminium alloy on the effect of pulsating water jet. Strojniški vestnik - Journal of Mechanical Engineering, 2017, Vol.63, No.10, pp 577-582. https://doi.org/10.5545/sv-jme.2017.4356

[Lehocka 2016] Lehocka, D., et al. Copper alloys disintegration using pulsating water jet. Measurement, 2016, Vol.82, pp 375-383. https://doi.org/10.1016/j.measurement.2016.01.014

[Lehocka 2018] Lehocka, D., et al. Pulsating water jet erosion effect on a brass flat solid surface. The International Journal of Advanced Manufacturing Technology, 2018, Vol.97, pp 1099-1112. https://doi.org/10.1007/s00170-018-1882-4

[Marzbali 2023] Marzbali, M., et al. Liquid–Solid Impact Mechanism, Liquid Impingement Erosion, and Erosion-Resistant Surface Engineering: A Review. Coatings, 2023, Vol.13, No.3, 577. https://doi.org/10.3390/coatings13030577

[McQueen 1986] McQueen, H.J., et al. Static recovery of copper during annealing and stress relaxation following hot deformation. Materials Science and Engineering, 1986, Vol.81, pp 355-369. https://doi.org/10.1016/0025-5416(86)90275-2

[Nag 2019] Nag, A., et al. Acoustic chamber length performance analysis in ultrasonic pulsating water jet erosion of ductile material. Journal of Manufacturing Processes., 2019, Vol.47, pp 347-356. https://doi.org/10.1016/j.jmapro.2019.10.008

[Nastic 2023] Nastic, A., et al. High speed water droplet impact erosive behavior on dry and wet pulsed waterjet treated surfaces. Physics of Fluids, 2023, Vol.35, No.5. https://doi.org/10.1063/5.0147698

[Poloprudsky 2021] Poloprudský, J., et al. Surface and subsurface analysis of stainless steel and titanium alloys exposed to ultrasonic pulsating water jet. Materials, 2021, Vol.14, No.18, 5212. https://doi.org/10.3390/ma14185212

[Poloprudsky 2022] Poloprudský, J., et al. Effects of liquid droplet volume and impact frequency on the integrity of Al alloy AW2014 exposed to subsonic speeds of pulsating water jets. Wear, 2022, Vol.488, 204136. https://doi.org/10.1016/j.wear.2021.204136

[Poloprudsky 2024] Poloprudský, J., et al. Water droplet erosion assessment in the initial stages on AISI 316 L using kernel average misorientation. Tribology International, 2024, Vol.191, 109165. https://doi.org/10.1016/j.triboint.2023.109165

[Poloprudsky 2024b] Poloprudsky, J., et al. Effect of technological parameters of the pulsating water jet on erosion effectivity on a linear trajectory. MM Science Journal, 2024. https://doi.org/10.17973/MMSJ.2024_10_2024073

[Reddy 1987] Reddy, A.V., et al. The influence of grain size on the erosion rate of metals. Metallurgical Transactions A, 1987, Vol.18, No.6, pp 1043-1052. https://doi.org/10.1007/BF02668553

[Ren 2023] Ren, M., et al. Evolutions of microstructure and mechanical properties of copper/SS304L composite micro channels during micro rolling. Materials Science and Engineering: A, 2023, Vol.871, 144881. https://doi.org/10.1016/j.msea.2023.144881

[Siahpour 2022] Siahpour, P., et al. Surface characteristics and residual stress generation in Ti-6Al-4 V following ultrasonic pulsed water jet peening. Surface and Coatings Technology, 2022, Vol.445, 128691. https://doi.org/10.1016/j.surfcoat.2022.128691

[Srivastava 2020] Srivastava, M., et al. Standoff distance in ultrasonic pulsating water jet. Materials, 2020, Vol.14, 88. https://doi.org/10.3390/ma14010088

[Stolarik 2023] Stolárik, G., et al. Assessment of surface irregularities created by controlled liquid droplet on the surface of stainless steel AISI 304L. Engineering Science and Technology an International Journal, 2023, Vol.47, 101558. https://doi.org/10.1016/j.jestch.2023.101558

[Stolarik 2024] Stolárik, G., et al. Submerged surface texturing of AISI 304L using the pulsating water jet method. Archives of Civil and Mechanical Engineering, 2024, Vol.24, 207. https://doi.org/10.1007/s43452-024-01029-x

[Stolarik 2025] Stolárik, G., et al. Ultrasonic pulsating water jet drilling-preliminary study. MM Science Journal, 2025. https://doi.org/10.17973/MMSJ.2025_03_2025005

[Svabenska 2020] Švábenská, E., et al. Effect of shock wave on microstructure of silicon steel, Surfaces and Interfaces, 2020, Vol.20, 100415. https://doi.org/10.1016/j.surfin.2019.100415

**[Thomas 1970]** Thomas, G. P., et al. Drop impingement erosion of metals. Proceedings of the Royal Society of London. A. Mathematical and Physical Sciences, 1970, Vol.314, pp 549-565. https://doi.org/10.1098/rspa.1970.0022

**[Zhang 2022]** Zhang, X., et al. Microstructure stability, softening temperature and strengthening mechanism of pure copper, CuCrZr and Cu-Al2O3 up to 1000 °C. Nuclear Materials and Energy, 2022, Vol.30, 101123. https://doi.org/10.1016/j.nme.2022.101123

**CONTACTS:**
Ing. Gabriel Stolarik, PhD.
Faculty of Manufacturing Technologies TUKE with a seat in Presov, Slovak Republic,
Bayerova 1, 080 01 Presov, Slovakia
gabriel.stolarik@tuke.sk, https://fvt.tuke.sk/